Highly Sensitive Detection of Hg^{2+} Based on Imprinting Sensor-Modified DNA

Wanping Dang, Yang Li, and Jingjing Zhang

***Abstract*—In order to enhance the sensitivity of the imprinted electrochemical sensor for detecting mercury ions, a novel ionimprinted electrochemical sensor modified with deoxyribonucleic acid (DNA) was proposed. A target imprinted with mercury ions was prepared using gold nanoparticles (AuNPs), mercury ion templates, and chitosan. Subsequently, a sensor imprinted with DNA was prepared by immobilizing DNA probes on the surface of AuNPs. The feasibility, electrochemical performance, and electrochemical reaction mechanism of the DNA-imprinted sensors were analyzed through experimental comparisons, scanning electron microscope (SEM), and kinetic studies. The working curve was obtained by the DPV method. The results show that the DNA-imprinted sensor achieves multiple signal amplifications through the unique coordination between Hg^{2+} and thymine (T) bases, as well as the formation of strong complexes between Hg^{2+} and chitosan molecularly imprinted polymers. The sensitivity of the DNA-imprinted sensor is significantly improved to 2.282×10^{-6} A·(uM)$^{-1}$. In addition, the exchange current density of the DNA-imprinted sensor is 5.793×10^{-8} A·cm^{-2}. The detection range was 10–60 nM with the detection limit of 1.62 nM (3σ/slope). The dynamics of DNA-imprinted sensor were analyzed. The proposed detection method provides theoretical and technical support for the detection application of Hg^{2+} and other ions.**

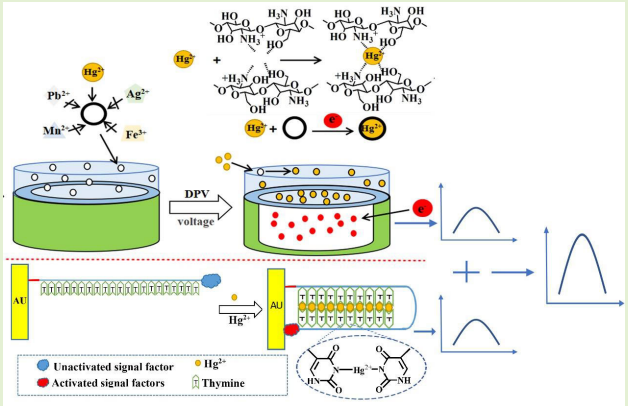

***Index Terms*— Deoxyribonucleic acid (DNA)-imprinted sensor, Hg^{2+} detection, high sensitivity.**

I. Introduction

HEAVY metal pollution poses a significant threat to the environment and human health. Among them, Hg^{2+} is highly toxic and persistent, and it could spread and accumulate globally through the atmosphere, water bodies, and the food chain. Long-term exposure to mercury could lead to severe health problems, including neurological damage, immune system disorders, and damage to the reproductive system [1]. Therefore, the development of highly sensitive and selective Hg^{2+} sensors is crucial for environmental monitoring and bioanalysis.

There are various methods for detecting trace heavy metal ions, including surface-enhanced Raman scattering (SERS) [2], atomic absorption spectroscopy (AAS) [3], inductively coupled plasma mass spectrometry (ICP-MS) [4], X-ray fluorescence spectroscopy (XRF) [5], and photoelectrochemical methods [6]. These methods have several limitations, including complex operating procedures, expensive equipment requirements, and the necessity for sample pretreatment [7]. Therefore, the search for a cheap equipment, fast, sensitive, and reliable method to detect Hg^{2+} remains an urgent need.

In recent years, ion-imprinted polymers (IIPs) have been utilized for ion detection because of their structural stability and high sensitivity [8]. Compared with the nonimprinted Hg^{2+} sensors proposed in most literature, the imprinting method has a lower detection limit in Hg^{2+} ion detection [9], [10]. Chitosan (CS) can form stable complexes with heavy metal ions due to its abundant functional groups, such as ammonium ions, and is used as a functional monomer for IIPs [11]. However, the conductivity of CS is relatively poor. To enhance the conductivity of CS, it is common to incorporate conductive materials, such as gold nanoparticles (AuNPs) [12]. Although IIPs has high structural stability, its selectivity is

Manuscript received 27 March 2024; revised 18 May 2024; accepted 27 May 2024. Date of publication 10 June 2024; date of current version 1 August 2024. This work was supported in part by the Natural Science Foundation of Hainan Province under Grant 222MS008 and in part by the Education Department of Hainan Province under Project Hnky2021-18. The associate editor coordinating the review of this article and approving it for publication was Prof. Li-Chia Jerry Tai. *(Corresponding author: Jingjing Zhang.)*

Wanping Dang and Yang Li are with the School of Information and Communication, Hainan University, Haikou, Hainan 570288, China (e-mail: 1491900635@qq.com; 918699@qq.com).

Jingjing Zhang is with the School of Tropical Agriculture and Forestry, Hainan University, Danzhou 571737, China (e-mail: 993958@hainanu.edu.cn).

This article has supplementary downloadable material available at https://doi.org/10.1109/JSEN.2024.3407528, provided by the authors.

Digital Object Identifier 10.1109/JSEN.2024.3407528

TABLE I
DNA SEQUENCE

Name	Sequence
Hg-DNAzyme	5'-HS-SH-TTT TTT TTT TTT TTT TTT TTT-Methylene Blue-3'

relatively poor. How to improve the selectivity and sensitivity of IIPs is a significant challenge.

Deoxyribonucleic acid (DNA) aptamers exhibit high selectivity and sensitivity in detecting metal ions, as specific bases or sites of DNA specifically bind to certain metal ions [13], [14]. Meanwhile, AuNPs can provide corresponding sites for DNA and are used in biosensors to immobilize DNA probes [15].

Based on the above analysis, this article recommends a novel DNA-imprinted sensor. Imprinted sensor was prepared using mercury ion templates and chitosan. AuNPs were electrodeposited onto the imprinted sensor surface, and then, DNA was immobilized on the surface of the AuNPs, creating a novel DNA-imprinted sensor. The electrochemical performance and surface microscopic scans of the DNA-imprinted sensors were analyzed. The dynamics of DNA-imprinted sensor have been explored.

II. MATERIALS AND METHODS

A. Materials and Equipment

Chitosan powder (CS, with high viscosity) and six-mercapto-1-hexanol (MCH) were purchased from Shanghai Maclyn Biochemical Company Ltd. Glacial acetic acid was purchased from Xilong Scientific Company Ltd. Sodium tripolyphosphate (STPP) was purchased from Shanghai Aladdin Biochemical Technology Company Ltd. Ethylenediaminetetraacetic acid (EDTA) was purchased from Guangzhou Saigu Bio-Technology Company Ltd. DNA (Hg^{2+}-DNAzyme) was purchased from SBS Genetech Company Ltd. All other reagents used were of analytical grade and did not require additional purification. Deionized water with a conductivity of 18.2 MΩ·cm was used to prepare all aqueous solutions in the experiments. Table I shows the sequence of the DNA.

B. Equipment and Parameters

The characterization of the sensor was conducted using a scanning electron microscope (SEM, Phenom Pharos G2, China). Electrochemical tests were conducted utilizing a CHI660E electrochemical analyzer with a conventional three-electrode system. The working electrode, reference electrode, and counter electrode used are glassy carbon, silver/silver chloride (Ag/AgCl), and foil wire, respectively.

The parameters of CV were the lowest potential of −0.8 V, the highest potential of 0.8 V, and the scanning rate of 0.05 V/s. The DPV parameters were the final voltage of 2.8 V, the initial voltage of −0.1 V, and the amplitude of 0.05 V. The Tafel parameters were the final voltage of 1 V, the initial voltage of −1 V, and the scanning rate of 0.01 V/s.

C. Pretreatment of GCEs

Glassy carbon electrode (GCE) was first polished using a microcloth soaked in alumina slurry made from 0.3- and 0.05-μm alumina particles to achieve a smooth surface. After polishing, the electrodes were cleaned with ultrasound and deionized water and dried in an oven at 65 °C for 10 min. The electrode was then immersed in a 0.5-M sulfuric acid solution and activated using cyclic voltammetry. The scanning range for cyclic voltammetry was from −0.3 to +1.3 V with the scan rate of 50 mV/s until a stable current–voltage curve was obtained. After activation, the electrode was rinsed with deionized water.

D. Preparation of Imprint Sensor

The chitosan solution was prepared by mixing 0.2-g chitosan powder with 20 mL of acetic acid at room temperature and stirring the mixture for 4 h. The process of chelation between chitosan and Hg^{2+} was commonly accomplished by establishing coordination bonds with multiple amino functional groups. Based on a molar ratio of four amino groups chelating one Hg^{2+} ($n(Hg^{2+}):n(CS) = 0.25$), the molar ratio of Hg^{2+} to CS was determined to be 1:33. The 30-μL 498.5-μM Hg^{2+} solution was added to 990-μL chitosan solution. The 30-μL 498.5-μM/L Hg^{2+} solution was combined with 990-μL chitosan solution. The obtained mixture was ultrasonically stirred for 2 h to obtain a CS/Hg^{2+} solution. The 0.367-g STPP was added to 10 mL of distilled water to prepare a crosslinking agent solution.

The 3 μL of the CS/Hg^{2+} composite suspension was transferred onto the GCE surface and dried at room temperature for 20 min to form the CS/Hg^{2+} composite film. The obtained electrode was then immersed in a crosslinking agent solution for 2 h, followed by rinsing with deionized water. Then, the electrode was electrodeposited in a solution containing 5-mM tetrachloroauric acid at the voltage of −1.2 V for 10 s, repeated four times. Next, the electrode was immersed in 0.5-mol/L EDTA solution by magnetically stirred for 2 h to remove the target template and obtain the imprinted sensor. Finally, after cleaning with deionized water and air drying, the imprinted sensor was obtained.

E. Preparation of DNA-Imprinted Sensor

The tube containing powdered DNA (Hg-DNAzyme) was centrifuged at a speed of 12 000 r/min for 3 min. The buffer (10 × PBS, pH 7.2–7.4) was added to the centrifuge tube to obtain 10-μM Hg^{2+}-DNAzyme solution. The Hg DNA enzyme solution was heated in a water bath at 95 °C for 5 min, then placed in a refrigerator at 0 °C for 5 min, and finally stored in a refrigerator at 5 °C. To facilitate a reduction reaction, 2-mM TCEP solution was introduced into the Hg-DNAzyme solution. The 3-μL Hg-DNAzyme solution was transferred onto the surface of the imprinted sensor. After drying in the air, the electrode was then immersed in MCH solution for 1 h to prepare the DNA-imprinted sensor.

III. RESULTS AND DISCUSSION

A. Characterization of Sensor

Scanning electron microscope (SEM) and energy-dispersive spectroscopy (EDS) were used to characterize the imprinted sensor and DNA-imprinted sensor, as shown in Figs. 1 and 2. Fig. 1(a) shows the small particles, while Fig. 1(b) shows

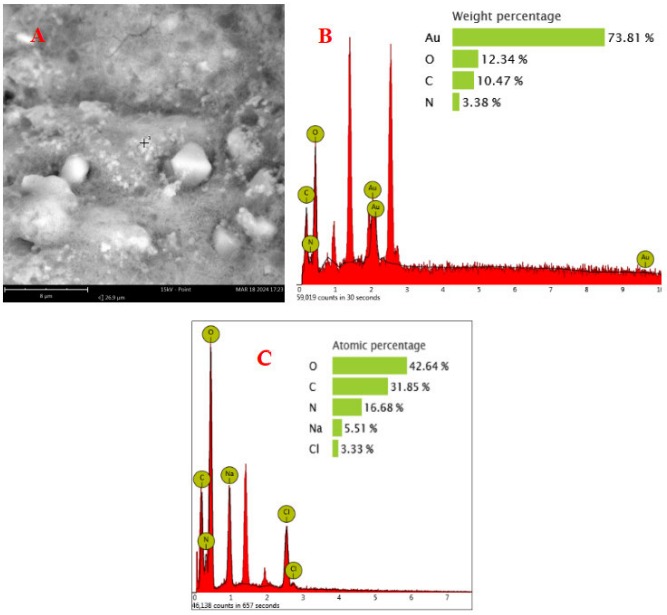

Fig. 1. Imprint sensor: (a) SEM, (b) EDS of particles, and (c) EDS of the entire graph.

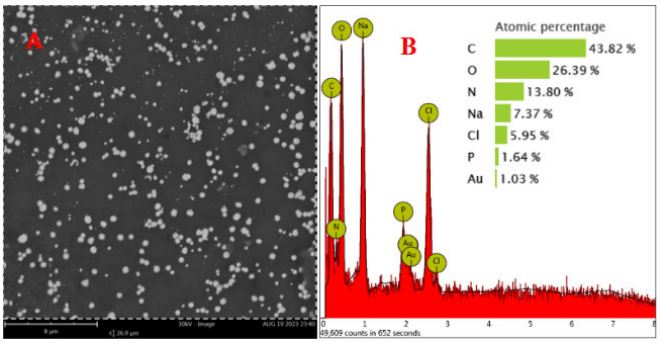

Fig. 2. DNA-imprinted sensor: (a) SEM and (b) EDS of the entire graph.

a Au specific gravity of 73.81%, indicating the successful preparation of AuNPs. Fig. 1(c) shows the presence of C, N, and O elements. The elements C, O, and N may all come from chitosan (CS). This indicates that the imprinted sensor has been successfully prepared. Compared with the imprinted sensor in Fig. 1, in addition to containing elements C, O, and N, there were also two elements of Au and P present in Fig. 2(b). The C, O, and N elements were mainly derived from chitosan and DNA. The P element was mainly derived from DNA. The Au element was obtained by electrodeposition of tetrachloroauric acid. This indicates that the DNA-imprinted sensor has been successfully prepared.

B. Preparation and Detection Principle of Sensors

Fig. 3 shows the preparation of a DNA-imprinted sensor and its principle for detecting Hg^{2+}. The imprinted sensor target was formed by mixing chitosan with Hg^{2+} template, crosslinking, electrodepositing gold nanoparticles (AuNPs), and removing the template. The target has a strong adsorption effect on Hg^{2+}, but weak adsorption on other ions. When target Hg^{2+} existed, the target adsorbed Hg^{2+}, resulting in an enhancement of the electrical signal. Meanwhile, single stranded DNA (Hg-DNAzyme) was composed

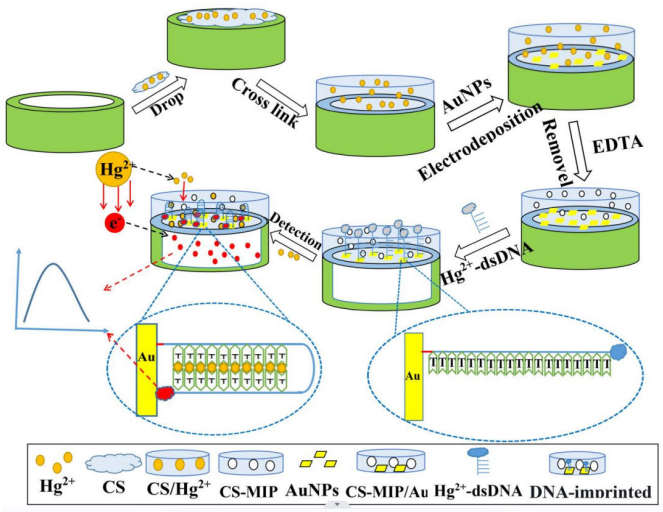

Fig. 3. Principle of DNA sensor.

of 21 thymine (T) bases, an S bond, and a signaling factor. Hg-DNAzyme was immobilized on the surface of AuNPs through S–Au bonds. The Hg^{2+} possessed the ability to selectively coordinate with thymine (T) bases, forming stable T–Hg^{2+}–T complexes. When Hg^{2+} was present, Hg-DNAzyme was formed into a hairpin shape through the T–Hg^{2+}–T structure. The signal molecule at one end of Hg-DNAzyme was approached by the electrode surface. Methylene blue signal molecule was a cationic phenothiazine dye, resulting in further enhancement of the electrical signal. Thus, the purpose of double signal amplification for detecting Hg^{2+} was achieved.

C. Feasibility Experimental Analysis

To explore the sensitivity of the DNA-imprinted sensor, electrodes modified with various materials were conducted by the differential pulse voltammetry (DPV), as shown in Fig. 4. The measurements were performed in 100-μM Hg^{2+} solution. The peak current of bare electrode, chitosan (CS)-modified electrode, and CS/Hg^{2+}-modified electrode was almost 0 A at 0–1.5 V, as shown in Fig. 4(a)–(c), respectively. The average peak current of the DNA sensor, imprinted sensor, and DNA-imprinted sensor was 7.591×10^{-5} A, 1.588×10^{-4} A, and 2.282×10^{-4} A, as shown in the yellow area of Fig. 4(d)–(f), respectively. The electrodes modified with different materials generate different peak currents, which preliminarily proves that DNA-imprinted sensor has been successfully prepared.

The calculation formula for sensitivity was $K = \overline{I}_p - \overline{I}_0 / C_{Hg^{2+}}$, where $\overline{I}_p$ was the average peak current of sensor, $\overline{I}_0$ was the average peak current of bare electrode, and $C_{Hg^{2+}}$ was the concentration of Hg^{2+}. The average sensitivity K was calculated, as shown in Table II (see Supporting Material Table S2 for the complete dataset). The average sensitivities of the DNA sensor, imprinted sensor, and DNA-imprinted sensor were 7.591×10^{-7} A/μM, 1.588×10^{-6} A/μM, and 2.282×10^{-6} A/μM, respectively. The average sensitivity of the DNA-imprinted sensor was significantly higher than that of the DNA sensor and the imprinted sensor. Compared with imprinted sensor, the sensitivity of DNA-imprinted sensor

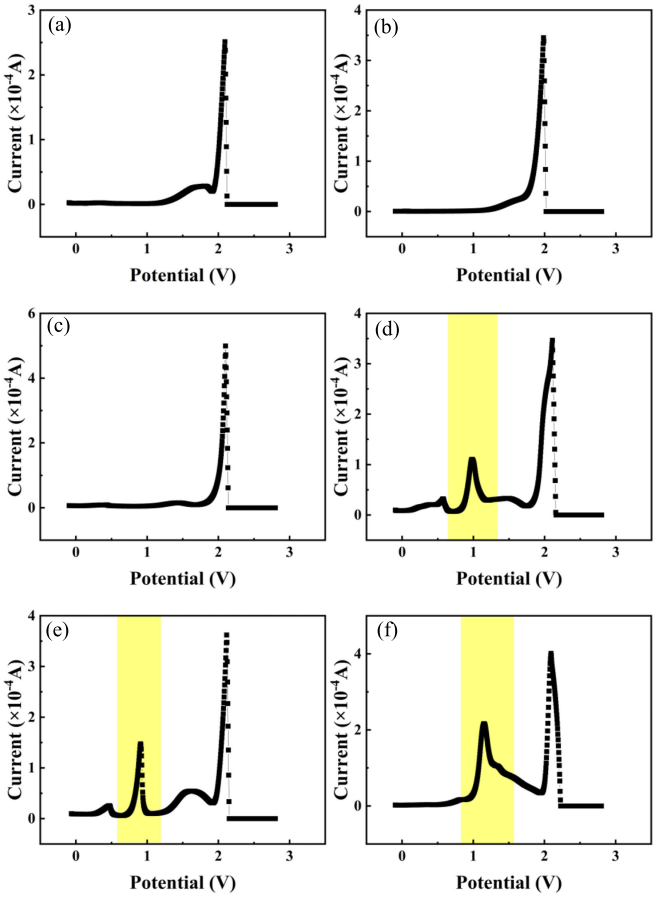

Fig. 4. Detection of 100-μM Hg^{2+} with different electrodes: (a) bare electrode, (b) CS-modified electrode, (c) CS/Hg^{2+}-modified electrode, (d) CS/Au-modified electrode, (e) imprinted sensor, and (f) DNA-imprinted sensor.

TABLE II
SENSOR SENSITIVITY

Name	$\overline{K}$(A/μM)
DNA sensor	7.591×10^{-7}
Imprinted sensor	1.588×10^{-6}
DNA-Imprinted sensor	2.282×10^{-6}

has increased by 43.70%. This confirms the feasibility of the recommended scheme shown in Fig. 3.

In order to further confirm the feasibility of the proposed scheme, an analysis was conducted from a dynamic perspective. Basic dynamic equation (Butler–Volmer)

$$i = \mathrm{FAK}^0\left[c_o(0,t)\exp\frac{-\beta F\left(E-E^{0t}\right)}{\mathrm{RT}} - c_R(0,t)\exp\frac{(1-\beta)F\left(E-E^{0t}\right)}{\mathrm{RT}}\right]. \quad (1)$$

In the equation, "i" represents the current density, "i_0" represents the exchange current density, "β" represents the transfer coefficient, "F" represents the Faraday constant, "R" represents the gas constant, "K" represents the reaction rate constant, "T" represents the reaction temperature, "E" denotes applied voltage potential, "E^{0t}" denotes standard potential, "c_o" represents the oxide concentration, and "c_R" represents the reductant concentration.

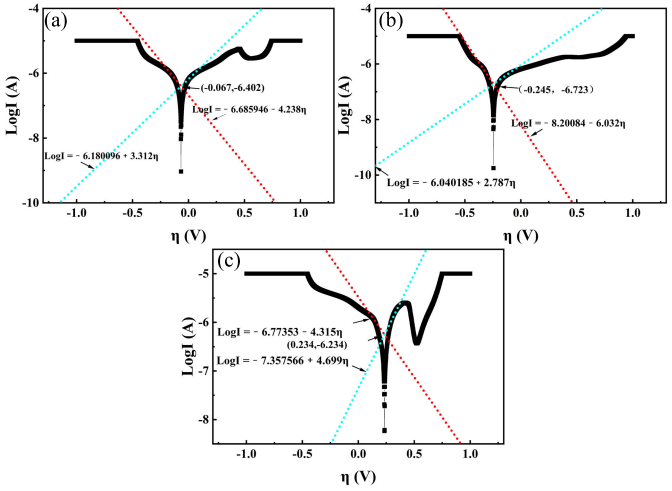

Fig. 5. Tafel lines: (a) DNA-imprinted sensor, (b) imprinted sensor, and (c) DNA sensor.

When the overpotential was large, such as in the case of a highly negative potential

$$i_0 = \mathrm{FA}k^0 c_o^{(1-\beta)} * c_R^{\beta}. \quad (2)$$

From (1) and (2), (3) could be derived

$$i = i_0\eta\left[\exp\frac{-\beta F}{\mathrm{RT}} - \exp\frac{(1-\beta)}{\mathrm{RT}}\right] \quad (3)$$

when the overpotential was large, such as in the case of a highly negative potential

$$\exp\frac{-\beta F}{\mathrm{RT}}\eta \gg \exp\frac{(1-\beta)}{\mathrm{RT}}\eta. \quad (4)$$

Thus, (4) could be simplified as follows:

$$i = i_0\exp\frac{-\beta F}{\mathrm{RT}}\eta. \quad (5)$$

Taking the natural logarithm on both sides and converting it into a logarithmic function with base ten, we got

$$\log i = \log i_0 - \frac{\beta F}{2.303\mathrm{RT}}\eta. \quad (6)$$

Equation (6) represented the theoretical model for the Tafel line in the strongly polarized region. Fig. 5 shows the Tafel curves obtained by detecting 100-μM Hg^{2+} with three-electrode materials (DNA-imprinted sensor, imprinted sensor, and DNA sensor). The Tafel line equation was obtained by fitting the strong polarization region. The alternating equilibrium current could be calculated using the theoretical model in (6), and the specific values were listed in Table III. According to Table III, the equilibrium exchange current for the DNA sensor was 1.554×10^{-7} A·cm^{-2}, and the imprinted sensor was 5.287×10^{-8} A·cm^{-2}. When the exchange current density value was low, the ability to resist deviation from equilibrium reactions was weaker, and polarization was more likely to occur. The imprinted sensor exhibited a smaller equilibrium exchange current compared to the DNA sensor, suggesting a higher level of polarization for the imprinted sensor. These results confirm the reason for the larger peak current of the

TABLE III
EXCHANGE CURRENT DENSITY

Name	$\overline{i_0}$ (A·cm^{-2})
DNA sensor	1.608×10^{-7}
Imprinted sensor	5.645×10^{-8}
DNA-Imprinted sensor	5.824×10^{-9}

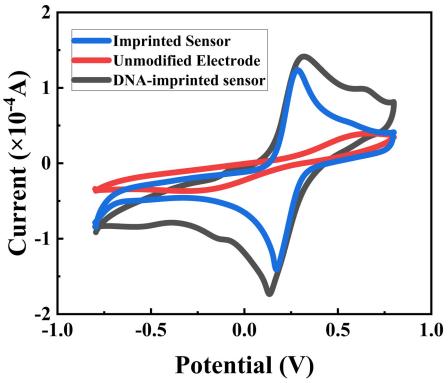

Fig. 6. Voltammetric curves of different sensors for detecting potassium ferricyanide.

imprinted sensor and the smallest peak current of the DNA sensor in the yellow area of Fig. 4(f). Compared with the equilibrium exchange current of imprinted sensors and DNA sensors, it was found that the equilibrium exchange current of DNA-imprinted sensors was the smallest with the value of 5.793×10^{-9} A·cm^{-2}. This indicated that the DNA-imprinted sensor had the strongest polarization, maximum peak current, and highest sensitivity. The results were consistent with those in Fig. 4 and Table II. This further confirms the viability of the designed approach.

In order to demonstrate the effectiveness of the DNA-imprinted sensor assembly, three different electrode materials (DNA-imprinted sensor, imprinted sensor, and DNA sensor) were used for DPV measurements of potassium ferrocyanide solution at a scan rate of 120 mV/s, as shown in Fig. 6. The unmodified electrode displayed the peak currents of -3.683×10^{-5} A and 3.915×10^{-5} A at the voltages of -0.311 and 0.645 V, respectively. The imprinted sensor exhibited higher peak currents at the voltages of 0.171 and 0.285 V in comparison with the unmodified electrode. The peak currents were -1.41×10^{-5} A and 1.237×10^{-4} A, respectively. The possible reason was that the imprinted sensor had a high porosity and surface area, which could increase the contact area between the electrode and electrolyte, enhance the reaction interface, and ultimately improve the peak current. The DNA-imprinted sensor exhibited the peak currents of 1.416×10^{-4} A and -1.735×10^{-4} A at the voltages of 0.319 and 0.139 V, respectively. Due to the use of phosphorus as the backbone in DNA, phosphorus carried electrons and had a strong adsorption effect on positive ions. At the same time, the ammonium functional group in the imprinting had a strong adsorption effect on ions. So, the redox peak current of DNA-imprinted sensors is higher than the redox score current of imprinted sensors and unmodified

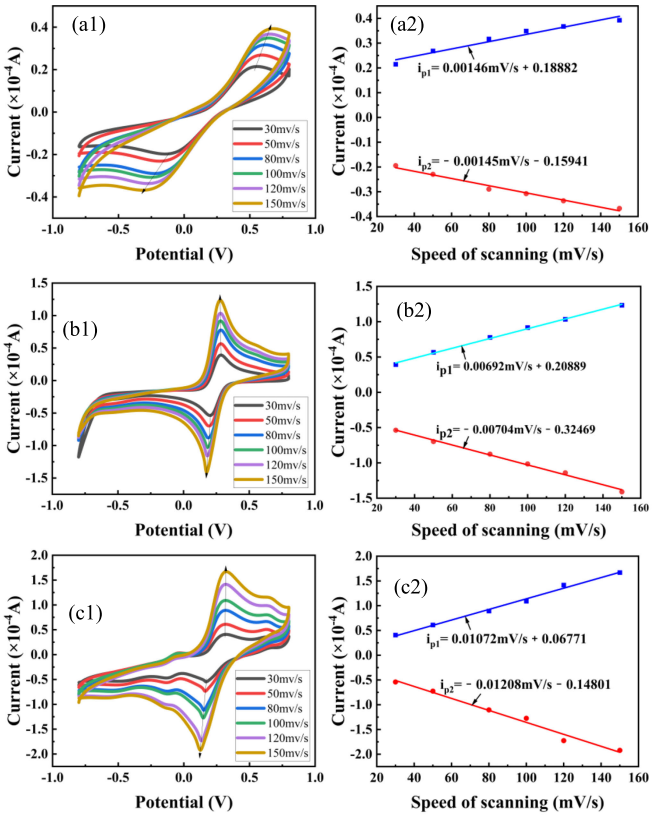

Fig. 7. Potassium ferrocyanide detection at different scanning speeds: (a1) CV curve of unmodified electrode, (a2) fitting line of unmodified electrode, (b1) CV curve of imprinted sensor, (b2) fitting line of imprinted sensor, (c1) CV curve of DNA imprinted sensor, (c2) fitting line of DNA imprinted sensor. Detection of potassium ferrocyanide with different sensors at different scanning speeds: (a1) unmodified electrode, (b1) imprinted sensor, (c1) DNA-imprinted sensor, (a2) unmodified electrode, (b2) imprinted sensor, and (c2) DNA-imprinted sensor.

electrodes. The comparative experiment suggests that the DNA-imprinted sensor was successfully prepared.

In order to determine the active regions of different electrodes, various working electrodes, including unmodified electrodes, imprinted sensors, and DNA-imprinted sensors, were analyzed. These electrodes were used to measure the electrochemical response of ferrocyanide at different scan rates. Cyclic voltammetry curves were then plotted for each electrode. The relationship between peak current and scan rate was plotted by extracting the peak currents for oxidation and reduction, as shown in Fig. 7. The oxidation and reduction peak currents of the three electrodes increase with the increase of scanning rate. The Randles–Sevcik equation was

$$i_p = 2.69 \times 10^5 A D^{\frac{1}{2}} n^{\frac{3}{2}} v^{\frac{1}{2}} C \tag{7}$$

where "i_p" represented the peak oxidation or reduction current, "n" was the number of electrons involved in the electrochemical reaction ($n = 1$ in this case), "A" was the active area of the electrode, "D" was the diffusion coefficient (at 25 °C, $D = 6.70 \times 10^{-6}$ cm^2/s), "C" was the electrolyte concentration ($C = 5$ mM), and "v" was the scan rate.

According to (7) and the oxidation peak current i_p values in Fig. 4(d)–(f), the active areas of the electrodes were calculated, as shown in Table IV. The active areas of unmodified electrode, imprinted sensor, and DNA-imprinted sensor were

TABLE IV
ELECTRODE ACTIVE AREA

Name	A(cm^2)
Unmodified electrode	0.957
Imprinted sensor	2.576
DNA-Imprinted sensor	3.259

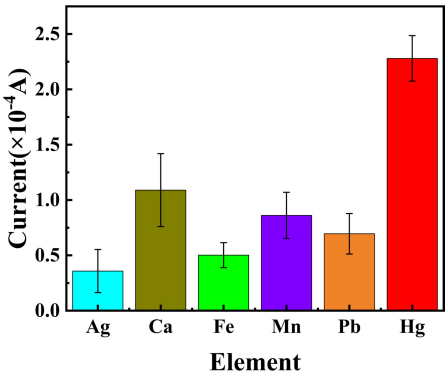

Fig. 8. Detection of different metal ions at a concentration of 100 μM/L using a DNA-imprinted sensor.

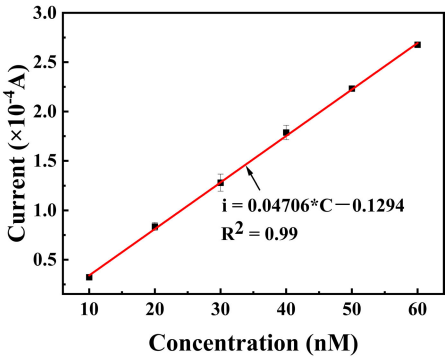

Fig. 9. Working straight line.

calculated to be 0.957, 2.576, and 3.259 cm^2, respectively. The DNA-imprinted sensor exhibited the largest effective area, while the unmodified electrode had the smallest effective area. This further confirms that the DNA-imprinted sensor has been successfully prepared, and the recommended scheme in Fig. 3 is feasible.

D. Selectivity Analysis

Fig. 8 represented the DNA-imprinted sensor detecting 100-μM solutions of Ag^+, Pb^{2+}, Fe^{3+}, Mn^{2+}, Ca^{2+}, and Hg^{2+} (see Supporting Material Fig. S4 and Table S4). Before testing, the DNA imprinting sensors were immersed in the tested liquid and incubated for 1 h. Compared with the peak current values of Ag^+, Pb^{2+}, Fe^{3+}, Mn^{2+}, and Ca^{2+} solution, it could be observed that the peak current of Hg^{2+} solution was significantly higher. These results indicate that the DNA-imprinted sensor has relatively high selectivity for mercury ions.

E. Linearity Analysis

To evaluate the linear performance of the sensor, different Hg^{2+} concentrations (10, 20, 30, 40, 50, and 60 nM) were tested, as shown in Fig. 9 (see Supporting Material Fig. S5 and Table S5). Before testing, the DNA imprinting sensors were immersed in the tested liquid and incubated for 1 h. The working curve is obtained through the DPV curve. The equation of the fitted line was $i = 0.04706$ C-0.1294. The detection limit was 1.62 nM (3σ/slope). Table V shows that DNA-imprinted sensors have lower LOD for Hg^{2+} detection compared to most literature.

TABLE V
COMPARISON OF DETECTION METHODS

Linear range	LOD	Reference
1-150 μM	60nM	[16]
0.3-700 nM	0.1 nM	[17]
0.25-250 μM	5.52nM	[18]
10-100 μM	3.42μM	[19]
1-100 μM	330 nM	[20]
15-50μM	15μM	[21]
5-5000μM	1.29μM	[22]
20-100μM	0.42μM	[23]
10-60 nM	1.62 nM	This work

TABLE VI
RECOVERY RATE OF Hg^{2+} IN TAP WATER

Hg^{2+} Added (nM)	Proposed method			
	Found (nM)	Recovery (%)	Standard Deviation (n = 3) (nM)	Relative Standard Deviation (n = 3) (%)
20	19.824 19.809 20.010	104.818	0.1119	0.5632
40	41.275 41.105 43.400	99.405	1.2788	3.0500
60	60.654 62.631 61.349	102.248	1.1112	1.81229

TABLE VII
RECOVERY RATE OF Hg^{2+} IN MILK

Hg^{2+} Added (nM)	Proposed method			
	Found (nM)	Recovery (%)	Standard Deviation (n = 3) (nM)	Relative Standard Deviation (n = 3) (%)
20	20.722 21.439 21.462	106.038	0.4208	1.9839
40	41.169 41.934 37.110	100.178	2.5927	6.4701
50	54.960 50.051 51.538	104.366	2.5172	4.8239

F. Recovery Rate of Hg^{2+} in Real Tap Water and Milk

The recovery rates in real tap water and milk were calculated, as shown in Tables VI (see Supporting Material Fig. S6 and Table S7) and VII (see Supporting Material Fig. S7 and Table S9), respectively. Tap water and pure milk were diluted to tenfold by buffer, respectively. Each sample was tested three times by DNA-imprinted sensor. In tap water, the range of recovery rate was 99.405%–104.818%, and the range of relative standard deviation (RSD) was 0.5632%–3.05%. In milk, the range of recovery rate was 100.178%–106.038%, and the

RSD range was 1.9839%–6.4701%. The results confirmed that the DNA-imprinted sensor has a very high recovery rate for detecting Hg^{2+} in tap water and milk.

IV. Conclusion

The study confirmed the successful synthesis of a new DNA-imprinted sensor using SEM, EDS, and electrochemical activity methods. Compared with traditional DNA sensors and imprinting sensors, the DNA-imprinting sensors have a lower exchange current density of 5.793×10^{-9} A·cm^{-2}, with a large active surface area of 3.259 cm^2, significantly increased sensitivity to 2.282×10^{-6} A·(μM)$^{-1}$. The detection range was 10–60 nM with the detection limit of 1.62 nM (3σ/slope). The dynamics of DNA-imprinted sensor were analyzed. The DNA-imprinted sensor demonstrated high sensitivity, selectivity, and recovery for detecting Hg^{2+}, providing theoretical and technical support for the detection application of Hg^{2+}.

References

[1] B. P. Panda et al. "Assessment of environmental and carcinogenic health hazards from heavy metal contamination in sediments of wetlands," *Sci. Rep.*, vol. 13, no. 1, p. 16314, 2023, doi: 10.1038/s41598-023-43349-7.

[2] L. Cui, P. Wang, Y. Fang, Y. Li, and M. Sun, "A plasmon-driven selective surface catalytic reaction revealed by surface-enhanced Raman scattering in an electrochemical environment," *Sci. Rep.*, vol. 5, no. 1, p. 11920, 2015, doi: 10.1038/srep11920.

[3] M. C. Greaves, "Determination of gold and of silver in solution by atomic absorption spectroscopy," *Nature*, vol. 199, no. 4893, pp. 552–553, 1963, doi: 10.1038/199552a0.

[4] R. Luo et al., "Determination of arsenic and lead in single hair strands by laser ablation inductively coupled plasma mass spectrometry," *Sci. Rep.*, vol. 7, no. 1, p. 3426, 2017, doi: 10.1038/s41598-017-03660-6.

[5] J. Wang et al., "In situ X-ray spectroscopies beyond conventional X-ray absorption spectroscopy on deciphering dynamic configuration of electrocatalysts," *Nature Commun.*, vol. 14, no. 1, p. 6576, 2023, doi: 10.1038/s41467-023-42370-8.

[6] Z. Ji et al., "A novel molecularly imprinted photoelectrochemical sensor utilizing Ag/SnO_2 for the highly sensitive and selective detection of 2,4-dichlorophenoxyacetic acid," *Microchemical J.*, vol. 200, Jul. 2024, Art. no. 110278, doi: 10.1016/j.microc.2024.110278.

[7] Z. Kang et al., "Electronic structure engineering of Cu_2O film/ZnO nanorods array all-oxide p-n heterostructure for enhanced photoelectrochemical property and self-powered biosensing application," *Sci. Rep.*, vol. 5, no. 1, p. 7882, 2015, doi: 10.1038/srep07882.

[8] L. Geng et al., "Molecularly imprinted electrochemical sensor based on multi-walled carbon nanotubes for specific recognition and determination of chloramphenicol in milk," *Microchemical J.*, vol. 182, Jun. 2022, Art. no. 107887, doi: 10.1016/j.microc.2022.107887.

[9] Y. S. Ridwan et al., "Review-towards mercury free: Ion imprinted polymer-based electrochemical sensors for monitoring of mercury(II)," *J. Electrochem. Soc.*, vol. 170, no. 12, 2023, Art. no. 127503, doi: 10.1149/1945-7111/ad0b46.

[10] J. E. Francisco et al., "Synthesis and application of ion-imprinted polymer for the determination of mercury II in water samples," *Environ. Sci. Pollut. Res.*, vol. 26, no. 19, pp. 19588–19597, 2019, doi: 10.1007/s11356-019-05178-y.

[11] A. Zhuolin et al., "Ion-imprinted polymers modified sensor for electrochemical detection of Cu^{2+}," *Nano*, vol. 13, no. 12, 2018, Art. no. 1850137.

[12] A. Bano et al., "Enhancing catalytic activity of gold nanoparticles in a standard redox reaction by investigating the impact of AuNPs size, temperature and reductant concentrations," *Sci. Rep.*, vol. 13, no. 1, p. 12359, 2023, doi: 10.1038/s41598-023-38234-2.

[13] C. D. Flynn et al., "Biomolecular sensors for advanced physiological monitoring," *Nature Rev. Bioeng.*, vol. 1, no. 8, pp. 560–575, 2023, doi: 10.1038/s44222-023-00067-z.

[14] F. Maâtouk et al., "An electrochemical DNA biosensor for trace amounts of mercury ion quantification," *J. Water Health*, vol. 14, no. 5, pp. 808–815, 2016, doi: 10.2166/wh.2016.293.

[15] J. Cui et al., "Facile synthesis of degradable CA/CS imprinted membrane by hydrolysis polymerization for effective separation and recovery of Li^+," *Carbohydrate Polym.*, 205, pp. 492–499, Feb. 2019, doi: 10.1016/j.carbpol.2018.10.094.

[16] A. Bilgic and Z. Aydin, "A new bodipy/pillar[5]arene functionalized magnetic sporopollenin for the detection of Cu(II) and Hg(II) ions in aqueous solution," *J. Colloid Interface Sci.*, vol. 657, pp. 102–113, Mar. 2024, doi: 10.1016/j.jcis.2023.11.147.

[17] R. Cao et al., "Detection of trace Hg(II) in cosmetics and aqueous solution by a gold nanospikes electrochemical sensor," *J. Electrochem. Soc.*, vol. 170, no. 3, 2023, Art. no. 037510, doi: 10.1149/1945-7111/acc0a1.

[18] N. M. H. El-Wakeel et al., "Chitosan-based fluorescein amphiphile macromolecular sensor for Hg^{2+} detection," *J. Mol. Liquids*, vol. 380, Jun. 2023, Art. no. 121744, doi: 10.1016/j.molliq.2023.121744.

[19] A. Bilgic, A. Cimen, M. Bayrak, and A. N. Kursunlu, "A new eco-friendly fluorescent microcapsules for effective and selective detection of Hg(II)&Cu(II)," *J. Photochemistry Photobiology A, Chem.*, vol. 448, Aug. 2024, Art. no. 115346, doi: 10.1016/j.jphotochem.2023.115346.

[20] A. Bilgic, A. Cimen, M. Bayrak, and A. N. Kursunlu, "Ultra-hybrid sensor based on magnetic and fluorescent biomaterial for the sensitive/selective detection of toxic Ag^+ and Hg^2+ ions in real samples," *Mater. Today Sustainability*, vol. 25, Feb. 2024, Art. no. 100696, doi: 10.1016/j.mtsust.2024.100696.

[21] N. A. Azmi, S. H. Ahmad, and S. C. Low, "Detection of mercury ions in water using a membrane-based colorimetric sensor," *RSC Adv.*, vol. 8, no. 1, pp. 251–261, 2018, doi: 10.1039/C7RA11450H.

[22] X. Jiang, H. Zhang, C. Yang, J. Xia, G. Liu, and X. Luo, "A novel electrostatic drive strategy to prepare glutathione-capped gold nanoclusters embedded quaternized cellulose membranes fluorescent colorimetric sensor for Pb(II) and Hg(II) ions detection," *Sensors Actuators B, Chem.*, vol. 368, Jul. 2022, Art. no. 132046, doi: 10.1016/j.snb.2022.132046.

[23] C. Kaewprom, Y. Areerob, W.-C. Oh, K. L. Ameta, and S. Chanthai, "Simultaneous determination of Hg(II) and Cu(II) in water samples using fluorescence quenching sensor of N-doped and N,K co-doped graphene quantum dots," *Arabian J. Chem.*, vol. 13, no. 2, pp. 3714–3723, 2020, doi: 10.1016/j.arabjc.2019.12.014.

Wanping Dang received the bachelor's degree in electronic science and technology from Hainan University, Haikou, China, in 2022, where he is currently pursuing the master's degree in electronic information with the School of Information and Communication Engineering.

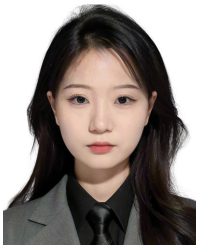

Yang Li received the bachelor's degree in Internet-of-Things engineering from Hainan University, Haikou, China, in 2022, where she is currently pursuing the master's degree in forestry.

Jingjing Zhang received the Ph.D. degree in information and communication engineering from Hainan University, Haikou, China, in 2019.

He is currently an Associate Professor with Hainan University and the Head of the Department of IoT Engineering and Network Engineering. His main research direction is the creation of sensors and IoT systems.